Nickel Isotope Fractionation As an Indicator of Ni Sulfide Precipitation Associated with Microbially Mediated Sulfate Reduction

Parigi, R., Pakostova, E., Reid, J. W., Saurette, E. M., McBeth, J. M., Ptacek, C. J. & Blowes, D. W.

DOI 10.1021/acs.est.2c00523
ISSN 0013-936X
ESSN 1520-5851

Publisher: American Chemical Society

Nickel isotope fractionation as an indicator of Ni sulfide precipitation associated with microbially-mediated sulfate reduction

Roberta Parigi[1,*], Eva Pakostova[1,2], Joel W. Reid[3], Emily M. Saurette[1], Joyce M. McBeth[4], Carol J. Ptacek[1] and David W. Blowes[1]

[1]Department of Earth and Environmental Sciences, University of Waterloo, 200 University Avenue West, N2L 3G1 Waterloo, Canada

[2]Centre of Sport, Exercise and Life Sciences, Institute for Health and Wellbeing, Coventry University, Priory Street

Coventry CV1 5FB, United Kingdom

[3]Canadian Light Source Inc., 44 Innovation Blvd, S7N 2V3 Saskatoon, Canada

[4]Department of Geology, University of Regina, 3737 Wascana Pkwy, S4S 0A2 Regina, Canada

▪ ABSTRACT

Microbially-mediated sulfate reduction is a promising cost-effective and sustainable process utilized in permeable reactive barriers (PRB) and constructed wetlands to treat mine wastewater. Laboratory batch experiments were performed to evaluate nickel (Ni) isotope fractionation associated with precipitation of Ni-sulfides in the presence of the sulfate-reducing bacterium (SRB) *Desulfovibrio desulfuricans* ^{T} (DSM-642). Precipitates were collected anaerobically and characterized by synchrotron powder X-ray diffraction (PXRD), scanning electron microscopy combined with energy-dispersive X-ray spectroscopy (SEM-EDS) and transmission electron microscopy (TEM). Solid-phase analyses showed the precipitates associated with bacteria attached to the serum bottle walls were characterized by enhanced size and crystallinity. Lighter Ni isotopes were preferentially concentrated in the solid phase, whereas the solution was enriched in heavier Ni isotopes compared to the input solution. This fractionation pattern was consistent with closed-system equilibrium isotope fractionation, yielding a fractionation factor of $\Delta^{60}Ni_{solid\text{-}aq} = -1.99‰$. The Ni isotope

fractionation measured in this study indicate multiple Ni reaction mechanisms occurring in the complex SRB-Ni system. The results from this study offer insights into Ni isotope fractionation during interaction with SRB and provide a foundation for the characterization and development of Ni stable isotopes as tracers in environmental applications.

Keywords: Nickel isotopes; remediation; SRB; sulfide precipitation; PRB.

Synopsis: Research on Ni isotopes as tracers in environmental systems is lacking. This study focuses on Ni isotope fractionation associated with microbially-mediated Ni removal from solution.

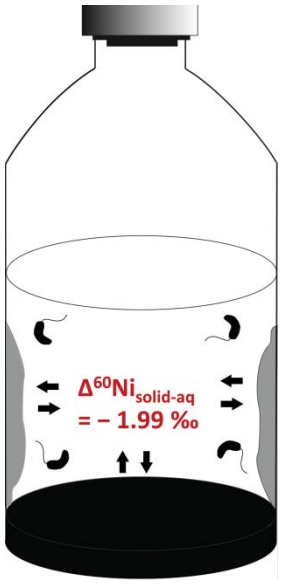

- **INTRODUCTION**

The extensive industrial use of Ni has led to the release of this metal into the environment[1]. Although Ni is considered an essential micronutrient for plants and many other organisms, high Ni concentrations can have harmful effects on plants, micro-organisms, animals, and humans[1-5]. Metal sulfide precipitation as a remediation technique has been successfully applied to treat acid mine drainage and industrial wastewaters and this approach has been shown to be more effective than traditional metal hydroxide precipitation[6,7]. The main advantages of sulfide precipitation include: the low solubility of sulfide phases, the high rate of removal at low pH, and the potential recovery of metals from the precipitates. Sulfide precipitates are also characterized by more rapid settling rates and improved dewatering properties compared to hydroxides[6,7]. Research involving Ni sulfide

precipitation at low temperature has included both biotic[8-13] and abiotic[14-19] experiments that have resulted in the formation of a variety of Ni sulfide phases, such as α-NiS, β-NiS, Ni_3S_4, NiS_2, Ni_3S_2, Ni_7S_6, Ni_9S_8, depending on the experimental conditions (i.e., pH, sulfur source, reaction time)[15,17-19]. Microbially-mediated reduction of sulfate under anaerobic conditions plays an important role in the treatment of waste streams contaminated by heavy metals[9-12,20]. Sulfate-reducing bacteria (SRB) can couple oxidation of organic matter with dissolved sulfate reduction (equation 1) resulting in metal attenuation through precipitation of metal sulfides (equation 2)[21]:

$$2CH_2O_{(s)} + SO_{4\,(aq)}^{2-} + 2H_{(aq)}^{+} \rightarrow H_2S_{(aq)} + 2CO_{2\,(aq)} + H_2O_{(l)} \quad (1)$$

$$Ni_{(aq)}^{2+} + H_2S_{(aq)} \rightarrow NiS_{(s)} + 2H_{(aq)}^{+} \quad (2)$$

In contrast with abiotic sulfide precipitation, the microbially-mediated process has the capacity to simultaneously remove dissolved sulfate and heavy metals, which are often problematic constituents in mining effluents and industrial wastewaters, at low cost and reduced risk[22]. Because of these aspects, SRB have been utilized with positive outcomes in passive remediation systems, such as permeable reactive barriers (PRBs)[21,23-25].

Metal stable isotope analysis has become a valuable tool in the field of environmental geochemistry with applications focussing on tracing the source and cycling of metals in the environment[26-32]. Despite this, Ni isotope measurements remain an under-exploited tool in environmental applications. Studies on Ni isotope fractionation conducted on microbial activity[33], types of vegetation[34,35], weathering[36-38], adsorption[39-43], and the formation of secondary minerals[39,40,44] have indicated that environmental processes induce significant Ni isotope fractionation, thus demonstrating the potential of Ni isotope analysis as a tool to trace Ni cycling in the environment. For example, recent studies have shown a preferential uptake of lighter Ni isotopes by minerals during adsorption onto calcite ($\Delta^{60}Ni_{min\text{-}aq} = -0.52‰$))[42] and birnessite ($\Delta^{60}Ni_{min\text{-}aq} = -2.76$ to $-3.35‰$)[43]. Furthermore, research involving the precipitation of Ni-hydroxide, Ni-

hydroxycarbonate, and Ni-sulfide has shown that lighter Ni isotopes are incorporated into the solid phases, resulting in fractionation factors ε = −0.40‰, −0.50‰, and −0.73‰, respectively[44]. Because Ni isotope signatures in environmental samples result from multiple Ni sources and transformation processes, Ni isotope tracing might be challenging. Laboratory experiments, focusing on the identification and quantification of Ni isotope fractionation associated with important biogeochemical processes, such as SRB-mediated sulfate reduction, are therefore crucial for the application of Ni isotopes as environmental tracers.

The purpose of this study was to determine the mechanisms responsible for Ni removal from solution under microbially-mediated sulfate reduction, and to measure Ni isotope fractionation associated with these processes. Assessment of Ni isotope signatures resulting from microbially-mediated attenuation of Ni in contaminated groundwater is of great importance for the application of isotope analysis to investigate the fate and bioavailability of Ni in the environment. Due to the important role SRB play in many passive remediation systems and in the natural environment, exploring their role is an important first step in understanding microbial processes influencing Ni isotope fractionation in mine-waste impacted systems.

- **MATERIALS AND METHOD**

Batch experiments. *Desulfovibrio* (*D.*) *desulfuricans*^{T} (strain Essex 6, DSM-642) was cultured in sterile Postgate B medium[45] which contained the following (per liter of distilled water): 0.5 g K_2HPO_4, 1.0 g $CaSO_4$, 1.0 g NH_4Cl, 2.0 g $MgSO_4.7H_2O$, 3.5 g Na lactate, 1.0 g yeast extract, 0.1 g ascorbic acid, 0.1 g thioglycolic acid, and 0.5 g $FeSO_4.7H_2O$. The medium was bubbled with argon (Ar) gas before the addition of $FeSO_4.7H_2O$. The pH of the complete medium was adjusted to 7.4 with 10 M NaOH. The medium (75 mL aliquots) was transferred to 100 mL serum bottles, and briefly bubbled with Ar. The serum bottles were capped (with butyl rubber septa) and crimped (with aluminium caps) before autoclaving (121 °C, 30 min). After cooling, the bottles were inoculated with *D. desulfuricans*, and incubated at room temperature for 6 days (without agitation) before subculturing (~10% inoculum) into fresh Postgate B medium.

Postgate C medium[45] containing in g L^{-1}: 0.5 KH_2PO_4, 1.0 NH_4Cl, 4.5 Na_2SO_4, 0.04 $CaCl_2 \cdot 2H_2O$, 0.06 $MgSO_4 \cdot 7H_2O$; 6.0 Na lactate, 1.0 yeast extract, 0.004 $FeSO_4 \cdot 7H_2O$, and 0.3 sodium citrate$\cdot 2H_2O$; pH~7.5, was transferred into 40 mL serum bottles and bubbled with Ar gas. The serum bottles were capped, crimped and autoclaved. Once cooled, the Postgate C medium was inoculated with the second-generation Postgate B culture (~1 mL) and incubated at 27°C (without agitation).

After several subcultures, 1 mL aliquots of *D. desulfuricans* at approximately late logarithmic phase (~24 h) were inoculated and cultivated at 27°C in 40 mL serum bottles filled with modified Postgate C medium (pH~6.8) that did not contain Fe or sodium citrate.

Filter-sterilized aliquots of 1M $NiCl_2$ stock solution, bubbled with Ar, were injected into the 40 mL serum bottles containing *D. desulfuricans* pre-grown in modified Postgate C medium for 4 days. Blank samples, composed of modified Postgate C medium, were analyzed before and after inoculation. The initial concentrations of Ni in solution were 10, 15, 20, 25, 30, and 40 mM. Sacrificial sampling was conducted at 1 hour, 1 day, and 1 week after the addition of Ni. Aqueous samples were filtered using 0.2 μm sterile syringe filters with Supor® Membrane (Acrodisc, Pall, UK), except for the subsamples on which pH measurement was performed. Samples for cation and Ni isotope analyses were acidified with concentrated HNO_3 (Omnitrace ultra, EMD Millipore). Total sulfur and Ni concentrations were analyzed by inductively coupled plasma optical emission spectrometry (ICP-OES; Thermo Scientific iCAP 6500). Solid samples were collected by centrifuging in an anaerobic chamber (N_2:H_2 with *ca* 1-3% H_2 atmosphere, Coy Laboratory Products Inc., Grass Lake, MI) to avoid oxidation. Solid subsamples for isotope analysis were washed multiple times with ultrapure water, frozen, freeze-dried, and digested with aqua regia. Subsamples for solid-phase characterization were also frozen and freeze-dried but not washed.

Parallel batch tests using the same conditions as adopted in the main experiment were conducted to evaluate the bacterial viability. After the exposure of SRB to the various Ni concentrations (10, 15, 20, 25, 30, and 40 mM) at the selected time intervals (1 hour, 1 day, and 1 week), 1 mL of solution was injected into a fresh Postgate B medium to assess the toxicity of Ni to the microorganisms. The

SRB viability was assessed by biomass production (turbidity) and inhibition of SRB growth was assessed by relatively lower (or absent) turbidity.

Isotope measurements. Sample preparation and Ni isotope analysis were conducted following Parigi et al., [44]. Briefly, acidified samples were spiked with a $^{61}Ni - {}^{62}Ni$ double-spike solution and purified following a two-step chromatography procedure. First, the samples were loaded onto anion exchange resin (Bio Rad AG MP-1M; 100–200 mesh, chloride form) to separate Ni from Fe, Zn and Cu. Afterwards, a Ni-specific resin (Eichrom Technologies) was used to ensure a clean sample. Eluted Ni fractions were evaporated and finally dissolved in 3% HNO_3 for MC-ICP-MS analyses. Nickel isotope ratios were determined on a Thermo Scientific Neptune MC-ICP-MS with an APEXQ desolvation introduction system (ESI). Measurements were made in high resolution mode on the low mass shoulders of the peaks to avoid polyatomic interferences. The raw data were processed following the method described by Siebert et al.[46], and the true isotopic composition of the samples was expressed as $\delta^{60}Ni$ in per mille (‰) relative to the NIST SRM 986 Ni isotope standard (equation 3):

$$\delta^{60}\mathrm{Ni} = \left[\frac{(^{60}\mathrm{Ni}/^{58}\mathrm{Ni})_{\mathrm{sample}}}{(^{60}\mathrm{Ni}/^{58}\mathrm{Ni})_{\mathrm{standard}}} - 1\right] \mathrm{x}\, 1000 \qquad (3)$$

Results were normalized to the average value of NIST SRM 986 determined before and after each sample. The long-term analytical reproducibility of the standard NIST SRM986 was determined to be ±0.05‰ (2SD, n = 167). A 2SD value of 0.05‰ (long-term reproducibility) was used when the 2SD related to three data points for each sample was <0.05‰. Procedural blanks were also included and subjected to the entire analytical procedure to evaluate possible contamination.

The external reproducibility was evaluated by measuring two reference materials, USGS Nod A1 and Nod P1. The measured $\delta^{60}Ni$ of 1.04 ±0.05‰ (n = 8), and 0.35 ±0.05‰ (n = 8) for Nod A1 and P1, respectively, agree with previously published data[36,40,47-49].

The measured Ni for the input solution $NiCl_2$ was -0.17‰ ± 0.05‰. For the purposes of plotting, comparison, and data interpretation, all samples were normalized to the input solution value ($\delta^{60}Ni_{NiCl2} = 0.00 \pm 0.05$‰).

Solid-phase characterization. Subsamples of the freeze-dried solid material were mounted in 0.5 mm ID polyimide capillaries (Cole-Parmer: 95820-04), which were sealed at both ends with gel adhesive (Loctite 454 Prism Gel, Henkel) and analyzed with synchrotron powder X-ray diffraction (PXRD). PXRD patterns were collected at the Canadian Light Source (CLS), Canadian Macromolecular Crystallography Facility (CMCF) bending magnet beamline (08B1-1)[50]. Two-dimensional (2D) diffraction data were collected on a Rayonix MX300HE detector, using a wavelength (λ) of 0.6888 Å (photon energy 18 keV). The sample-detector distance, detector centering, and tilt were calibrated using a lanthanum hexaboride (LaB_6) standard reference material (NIST SRM 660a LaB_6). The PXRD patterns were calibrated and integrated (2 to 40°, 2θ) using the GSASII software package[51]. Search/match phase identification was performed with Powder Diffraction File, PDF-4+ software[52].

Samples for whole-grain mounts were filtered with a Whatman® grade 4 (20 – 25 μm) cellulose filter to collect the precipitates for scanning electron microscopy and energy-dispersive X-ray spectroscopy (SEM-EDS) analyses. The precipitates were dried in an anaerobic glovebox (N_2 and H_2 (~1.5%) atmosphere) for approximately 24-hr and then dispersed on conductive carbon tape applied to a metal sample stub. All sample preparation was completed in an anaerobic chamber to prevent the oxidation of the precipitates, which contained reduced sulfur and metal phases. Mounted samples were removed from the anaerobic chamber in sealed containers and opened immediately before SEM analysis. Conductive coatings were not applied to whole-grain mount samples before analysis.

Grain mounts were characterized with a FEI Quanta™ 250 FEG-ESEM with an Oxford Instruments X-act silicon drift detector (SDD) for EDS. Back-scattered electron (BSE) and secondary electron

(SE) images were acquired with an accelerating voltage of 20 kV and a sample distance of 10 mm from the detectors.

Samples for transmission electron microscopy (TEM) characterization were sonicated to disperse the precipitated nanoparticles in solution and then diluted 1:100 in ultrapure water (MilliQ A10 water system 18.2 MΩ cm at 25 °C). The diluted solution was pipetted on to a Formvar/Carbon 400-mesh copper Pelco® TEM grid. Nanoparticles were characterized with a Zeiss Libra 200MC TEM equipped with an EDS detector. TEM images were acquired at an accelerating voltage of 200 kV. Images were processed using Digital Micrograph (Gatan Inc.) and lattice distances were calculated from the inverse fast Fourier Transform (FFT) patterns of selected areas after masking the FFT pattern to improve the delineation of atomic distances.

- **RESULTS AND DISCUSSION**

Nickel removal by SRB culture. Results from the batch experiments are summarized in the Supporting Information (Table S1). The pH values were characterized by a slow decrease over the course of the experiment: from initial values of 6.8, to final average values of 5.7 after a week (Table S1). The Ni removal efficiency achieved using different initial metal concentrations is shown in Figure S1. Nickel removal from solution reached almost 95% after 1 week in the batches with the lowest initial Ni concentration (10 mM). As the concentration of the Ni addition in the batch experiments increased, the extent of Ni removal progressively declined. The batches with the highest initial Ni concentration (40 mM) showed removal of approximately 25% of the initial Ni after 1 day. This removal remained relatively constant in the 1-day and 1-week samples likely due to the inhibition of the SRB by the high metal concentration. Bacterial viability tests showed no bacterial growth in fresh Postgate B inoculated from the batches containing 40 mM of Ni and sampled after 1 day and 1 week. These results confirmed the negative impact of the highest Ni concentration used in the experiments (40 mM) on the SRB.

Total sulfur concentrations in solution also decreased with time, showing a removal of ~50% after 1 week, common to all the batches regardless of the initial Ni amounts.

Characterization of the solid phase. The final solid phase products were composed of a predominant black precipitate that accumulated at the bottom of the serum bottles and thin sheets of a precipitate with a metallic lustre that formed on the walls of the bottles (Figure S2 a, b, and c). The precipitate with the metallic lustre increased over the course of the experiments, and its growth was inversely proportional to the initial concentration of Ni. The 10 mM Ni samples had the largest amount and the 40 mM Ni samples had only a small amount of this solid phase. The solid-phase formation and resulting solid composition were likely affected by the composition of the SRB growth medium (inorganic constituents in particular). However, the environmental conditions in mine remediation systems such as PRB can vary significantly based on a plethora of factors (such as PRB composition and age as well as the mine effluent composition, hydrogeology of the site, climatic conditions etc.), thus complicating creating a representative experimental system.

During the experiments, the metallic precipitate formed first on the walls of the serum bottles, and subsequently accumulated at the bottom. At equal Ni concentrations, the 1-week samples showed the largest amount of this precipitate except for the 40 mM batches which displayed an equal amount of the same precipitate at collection times of 1 day and 1 week.

Due to the delicate, thin, sheet-like nature of this phase, it was impossible to effectively separate it from the black precipitates. Thus, samples taken for the solid product characterization consisted of a mixture of these two solid phases. The powder X-ray diffraction patterns for the 10 mM and 40 mM samples collected after 1 hour, 1 day, and 1 week are displayed in Figure 1. All patterns were characterized by broad peaks at ~14 degrees (d = ~ 2.8 Å) and ~22 degrees (d = ~1.8 Å). Similar features were also reported by previous abiotic[14,15,44] and biotic[10,13] Ni sulfide precipitation studies and were attributed to poorly crystalline polyphasic Ni-sulfide precursors[13]. Such poorly crystalline Ni sulfides were dominantly nanoparticulate material with the general formula $NiS{\cdot}1.5H_2O$ which displayed an anhydrous core of crystalline millerite (β-NiS) surrounded by a hydration shell[14]. The Ni:S ratio of the hydrated NiS exhibited a slight excess of Ni over S, thus indicating the potential deposition of a $Ni(OH)_2$-like phase in the mantle layer[53]. Some of the early time patterns (i.e., 10

mM at 1 hour, Figure 1Aa; 10 mM and 40 mM at 1 day, Figures 1Ba and 1Bb) showed an additional broad peak at ~8.5 degrees (d =~4.6 Å). As 4.6 Å corresponds to the Bragg reflection associated with the (001) planes of the mineral theophrastite ($Ni(OH)_2$), the presence of this peak is consistent with the potential precipitation of either a $Ni(OH)_2$-like phase or a hybrid material composed of both millerite and theophrastite structural components[53]. Furthermore, Wilkin and Rogers[16] demonstrated that freshly precipitated nickel sulfide is characterized by residual Ni-O coordination which is replaced by Ni-S coordination with ageing time.

Although the 1-day 10 mM and 1-day 40 mM patterns (Figures 1Ba and 1Bb) were also characterized by numerous Bragg reflections in addition to the broad features previously indicated, no conclusive matches were identified for most of these peaks. These two samples appeared to share a low angle reflection at ~ 4.22 degrees (d = ~ 9.4 Å), but most of the other low angle reflections were not common to both patterns. We therefore suggest that the 1-day samples may be composed of a mixture of metastable phases that were not well characterized in previous studies. Most of the peaks observed in the 1-day patterns were not visible in the 1-week patterns, confirming the metastable nature of the 1-day precipitates.

The 1-week patterns (Figure 1Ca and 1Cb) and all the 40 mM samples displayed halite (NaCl) Bragg reflections; this is presumed to be from residual salts from the media. In addition to this, the 1-week 40 mM sample was also characterized by the presence of nickelboussingaultite $(NH_4)_2Ni(SO_4)_2(H_2O)_6$ plus additional un-matched reflections, whereas the 1-week 10 mM sample showed sharp reflections due to thenardite (Na_2SO_4). Lattice parameters for nickelboussingaultite were slightly different from the reference PDF database entry (PDF 04-007-5461), due to either a different hydration state or slightly different ionic substitution. It is worth noting that the 1-week 10 mM diffraction pattern displayed sharper features associated with modifications of the poorly-crystalline NiS precursor (red asterisks in Figure 1Cb). These features were particularly accentuated at ~ 13.41 degrees (d ~ 2.95 Å) and ~ 23.37 degrees (d ~ 1.70 Å). No single nickel sulfide with peaks corresponding to both the 2.95 Å and 1.70 Å d-spacing was found. Polydymite [more intense

reflections (311) and (440) at 2.87 Å and 1.68 Å, respectively] and α-NiS [reflections (100) and (110) at 2.98 Å and 1.72 Å, respectively] were phases that displayed the most similar patterns (Figure 1Ca). The presence of these "sharper" peaks may indicate evolution from a poorly crystalline NiS precursor towards the development of higher-order Ni sulfides with time. In similar experiments, Mansor et al.[13] observed a distinct increase in crystallinity of biogenic Ni sulfide nanoparticles over a period of ~6 days, furthermore, the biogenic reaction products were characterized by enhanced dimensions and crystallinity relative to their abiogenic counterparts[13]. Similar findings were reported for SRB-mediated Zn sulfide formation[54]. The development of more crystalline phases associated with biotic precipitation of sulfides has been linked to the formation of a low pH micro-environment around the bacterial cell walls and to the presence of organic compounds secreted by SRB[13]. Conversion of Ni monosulfide to polydymite and vaesite has shown to be redox dependant[13,16], and, under anaerobic conditions, H^+ is the most probable oxidant to drive this transformation[55]. Consequently, the micro-environment around the bacteria cell walls, which differ chemically from the bulk circumneutral pH experimental conditions, could favour the precipitation of Ni sulfide minerals, such as polydymite and vaesite[13], favoured under low pH ($pH \leq 5$). Although vaesite is considered to be the most thermodynamically stable phase at low temperature[16], polydymite and vaesite reflections, which were clearly identified in the 10 mM 1-day powder X-ray diffraction pattern, were no longer present in the 10 mM 1-week sample.

All the 40 mM powder X-ray diffraction patterns displayed broad, low angle reflections at ~2.25 degrees (d ~ 17.5 Å) and ~3.65 degrees (d ~ 10.8 Å). These reflections, which were probably from the same phase due to comparable broadening and intensity ratios, had similarities with the patterns of clays, although no obvious matches were found in the PDF database. Bacterial microcolonies are known to mediate the formation of clay minerals[56-58]. Formation of colloidal clay-like phases (often Fe-bearing aluminosilicates) is favoured by the presence of bacteria and their metabolic products[58], and these poorly crystalline precursors may convert to more ordered phases over time[56-58]. The

presence of material with clay-like composition was observed through SEM-EDS analysis (Fig. S3).

SEM-EDS analyses performed on both the freeze-dried and freshly sampled 10 mM and 40 mM 1-week solid materials also showed that the larger grains, predominantly occurring as the precipitate with a metallic lustre, were made of aggregates of Ni sulfides with different habits and composition (Figure S4 to S6), which is consistent with the PXRD results. These higher-order aggregates were closely associated with bacteria attached on the serum bottle walls. Attached cells can form biofilms, which are microbial multicellular aggregates, that attach to surfaces and can often immobilize metal ions[55]. Although bacterially mediated sulfate-reduction by SRB was the main process responsible for Ni removal from solution in the present study, extracellular polymeric substances (EPS) secreted by bacterial cells can bind Ni and other metals, thus creating additional nucleation sites[10,13,60]. The SEM-EDS analysis of *D. desulfuricans* in our study showed Ni-sulfide precipitates surrounding the microorganisms (Figure S7). Precipitation of metal sulfides on bacterial surfaces is known to provide protection to SRB, enhancing their tolerance to the toxic effects of heavy metals[61]. Other studies indicate that metal nanoparticles can enhance electron uptake across the cell membrane enabling the bacteria to utilize solid-phase electron donors, as observed for Fe nanoparticles[62,63]. Chemotaxis and substrate storage are other speculated roles of metal nanoparticles in microbial metabolism[63].

The finest fraction of the solids mainly occurred as black precipitates that accumulated at the bottom of the bottles. Lattice-fringe spacing measurements, derived from the TEM study, confirmed the polycrystalline nature of these precipitates (Figure S8 A and B).

Although the final experimental batches were filled with a modified medium without Fe, SEM-EDS results indicated a small amount of Fe was carried over from previous batches during subculturing, and Fe had coprecipitated with and/or substituted Ni in the solid phase (Figure S6).

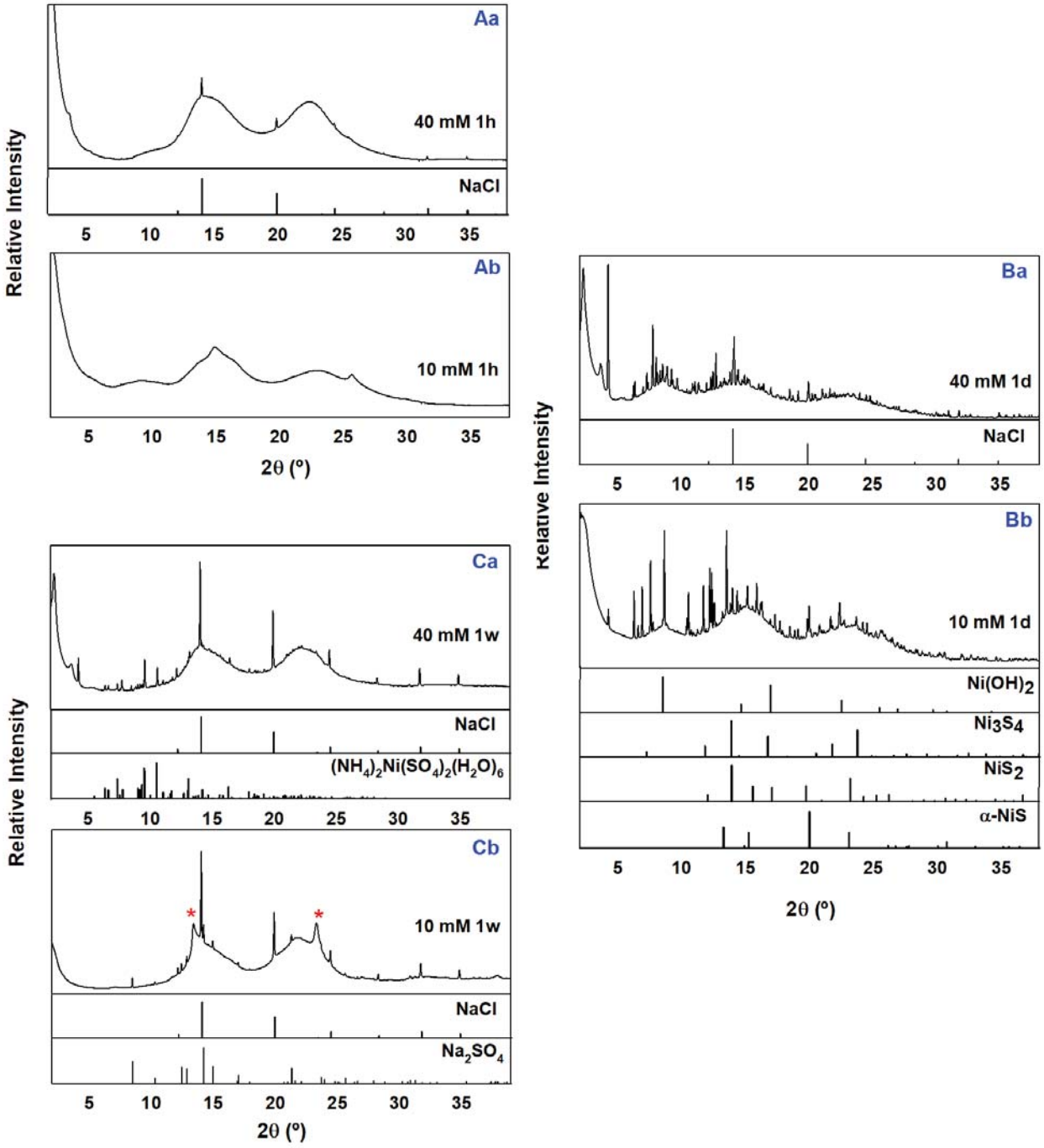

Figure 1: X-ray diffraction patterns of Ni precipitates: Aa) 40 mM Ni solid sample collected after 1 hour. Halite, NaCl (04-016-2944) Ab) 10 mM Ni solid sample collected after 1 hour. Ba) 40 mM Ni solid sample collected after 1 day. Halite, NaCl (04-016-2944) Bb) 10 mM Ni solid sample collected after 1 day. Theophrastite, $Ni(OH)_2$(04-013-3641), polydymite, Ni_3S_4 (04-004-5623), vaesite, NiS_2 (04-003-1992), α-NiS (04-002-6886). Ca) 40 mM Ni solid sample collected after 1 week. Halite, NaCl (04-016-2944), nickelboussingaultite, $(NH_4)_2Ni(SO_4)_2(H_2O)_6$ (04-007-5461). Cb) 10 mM Ni solid sample collected after 1 week. Halite, NaCl (04-016-2944), thenardite, Na_2SO_4 (04-010-2457). Red asterisk (*) indicates peaks corresponding to modifications of the poorly crystalline NiS precursor.

Isotope fractionation. The magnitude of Ni isotope fractionation between Ni in solution and Ni associated with the solid phase was investigated by varying the initial concentrations of Ni in solution. The isotope results are reported in Table S1.

Figure 2 displays the measured $\delta^{60}Ni$ values corresponding to the fractions of Ni in solution and in the associated solid phases. The isotope data were fitted with both reversible equilibrium and Rayleigh fractionation models. The black solid lines are the linear best-fit to the data, whereas the black dashed curves are the best-fit Rayleigh trends $\varepsilon = -1‰$ (Fig. 2). According to these results, the data seem to be best represented by equilibrium, closed-system fractionation (linear trends) with continuous exchange between the aqueous and the solid pools. An average magnitude of $\Delta^{60}Ni_{solid\text{-}aq} = -1.99‰$ was determined for the data set.

The data showed partitioning of light Ni isotopes in the solid phase compared to the initial solution, and enrichment in heavy isotopes of the residual aqueous Ni fractions. Enrichment in the heavier isotope associated with the aqueous fraction of Ni was observed in abiotic Ni sulfide precipitation experiments[44]. Isotopic fractionation in abiotic NiS precipitation experiments was fit with a Rayleigh curve yielding a fractionation factor of $\varepsilon = -0.73‰$[44]. Fujii et al.[64,65] also observed that lighter Ni isotopes preferentially partition into the sulfide species, reporting the equilibrium fractionation factors between the dissolved species Ni^{2+} and $Ni(HS)^{+}$ as $\Delta^{60}Ni_{Ni2+\text{-}Ni(HS)+} = + 0.68‰$ and $\Delta^{60}Ni_{Ni2+\text{-}Ni(HS)+} = + 0.66‰$ at 25°C, respectively. Vance et al.[66] reported a fractionation factor of −0.7 ‰ associated with the removal of dissolved Ni as Ni sulfidized species in the Black Sea at a depth ≥ 300 m.

The difference between the fractionation factors measured in this study and the magnitude of Ni isotope fractionation of ~ −0.7 ‰ calculated in other NiS precipitation studies[44, 64-66] can be quite surprising. However, it is important to note that, due to the complexity of the current experimental system, it is not possible to attribute the magnitude of the isotopic fractionation measured in this study to a single Ni sulfide precipitation process. Although Ni precipitation as sulfide phases was the main mechanism of Ni removal from solution, it is likely the fractionation measured in our

experiments resulted from a combination of multiple Ni attenuation processes present in the SRB system. As previously discussed, bacteria cell walls and EPS can bind heavy metals such as Ni, thus providing precipitation sites for metals and sulfide phases. Interactions between SRB and Ni might induce Ni isotope fractionation before the precipitation of sulfide phases occurs. Adsorption of dissolved Ni to the freshly precipitated Ni sulfides can also considerably affect the measured Ni isotope fractionation[44]. Ni adsorption to minerals was documented to cause enrichment of heavy Ni isotopes in solution compared to the solid phases and to generate significant Ni isotope fractionation[39-43]. For example, in a recent study, adsorption of Ni to the mineral birnessite induced the largest fractionation factors observed for Ni to date ($\Delta^{60}_{\text{min-aq}}$ ranging from −2.76‰ to −3.35‰)[43]. Nickel adsorption to and coprecipitation with clay-like phases, whose bio-induced formation was detected in the experiment, might also contribute to the measured isotope fractionations.

The reduced partition function ratios of $^{60}Ni/^{58}Ni$ ($10^3 \ln \beta_{60-58}$) related to important Ni sulfides calculated by Liu et al.[67] showed a decrease in the order of polydymite > heazlewoodite > millerite > godlevskite > vaesite, highlighting the connection between Ni isotope fractionation and Ni-S, Ni-Ni bond lengths of Ni sulfide crystals. Furthermore, Liu et al.[67] estimated the influence of Fe substitution on equilibrium Ni isotope fractionation in Ni sulfide minerals. Fe substitution for Ni yielded a decrease of the reduced partition function ratios of $^{60}Ni/^{58}Ni$. Thus, the presence of low concentrations of Fe, a characteristic of the current experimental systems, cannot be ignored, because changes in the Fe/Ni ratio can have a considerable influence on Ni isotope fractionation[67].

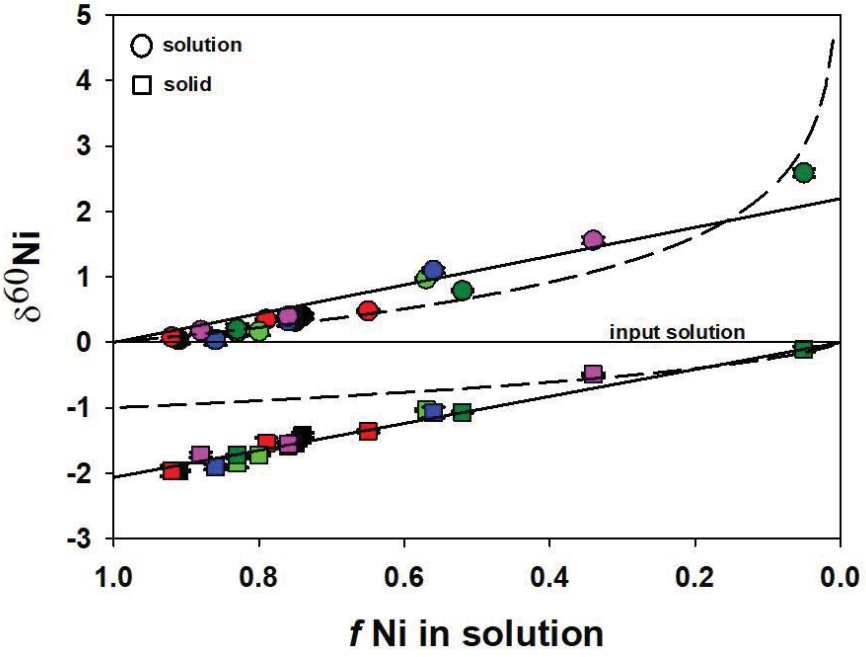

Figure 2: Ni (δ^{60}Ni) isotope fractionation relative to the input solution Ni concentration versus the fraction of Ni remaining in solution (f). The black straight lines represent the closed-system equilibrium fractionation trends yielding $\Delta^{60}Ni_{solid\text{-}aq}$ = −1.99‰; The dash curves are Rayleigh trends for ε^{60}Ni = −1‰. Black symbols correspond to the 40 mM samples; Red symbols correspond to the 30 mM samples; Light green symbols correspond to the 25 mM samples; Blue symbols correspond to the 20 mM samples; Pink symbols correspond to the 15 mM samples; Dark grey symbols correspond to the 10 mM samples. The error bars represent 2SD from three analytical measurements.

Environmental implications. The determination of fractionation factors of important biogeochemical processes, such as microbially-mediated sulfate reduction, is necessary to apply Ni isotopes as tracers for Ni sources and cycling in the environment. This study, which focused on the investigation of Ni fractionation associated with the mechanisms of Ni removal from solution occurring during Ni-SRB interactions. This is among the first studies to explore the potential of Ni isotopes as environmental tracers, offering an important addition to the existing literature, and providing a basis for further progress of Ni stable isotope analysis aimed to understand transport and fate of Ni in the environment.

Due to the close interaction between SRB and dissolved metal ions, SRB-based metal precipitation approaches are considered a valuable tool in passive treatment remediation. Because of the complexity of the investigated system, which is characterized by a multiplicity of mechanisms involved in the bio-mediated attenuation of Ni, it is challenging to attribute the measured fractionation factor to a single process. As a result, it is reasonable to ascribe the extent of

fractionation measured in the present study to a combination of mechanisms involved in removal of Ni from solution accompanied by formation of Ni-S phases. Additionally, bacterial activity is influenced by changes in geochemical and physical parameters, such as pH, nutrient availability, and dissolved oxygen concentration[59]. Interactions with complex microbial communities (in contrast to pure cultures such as the one used in the present study) may also result in differences in the isotopic signatures. Therefore, future studies that would aim to determine Ni isotope fractionation under varying experimental conditions would be beneficial to elucidate what mechanisms have the greatest impact on Ni isotope signatures in SRB systems and in more complex microbial communities.

- **ASSOCIATED CONTENT**

Concentration and isotope data derived from the precipitation experiments; fraction of Ni remaining in solution (f) vs. sampling time plot; pictures of the precipitate with metallic lustre; SEM and TEM images of the solid phase.

- **AUTHOR INFORMATION**

Corresponding Author

*E-mail; rparigi@uwaterloo.ca

Notes

The authors declare no competing financial interest.

- **AKNOWLEDGMENTS**

We acknowledge assistance provided by: Joy Hu, Laura Groza, Filip Budimir, Joanne Angai, Justin Buis (UWaterloo); Denis Spasyuk (CLS); Colton Vessey, James Schulte, and Matt Lindsay (USask). The authors would also like to acknowledge Dr. Kam Tong Leung's WatLAB facility (http://www.WATLab.com) and especially Dr. Lei Zhang and Dr. Nina F. Heinig for SEM training and assistance, and Dr. Joseph P. Thomas for operating the TEM. This project was funded by a Natural Sciences and Engineering Research Council (NSERC) Strategic Project Grant (NETGP 479708-15; D. Blowes, Principal Investigator), an Ontario Research Fund-Research Excellence

grant (RE09-061; awarded to D. Blowes, C. Ptacek and R. Amos), and an NSERC Discovery Grant (RGPIN-2019-07118; awarded to D. Blowes). Portions of the research described in this paper were performed at the Canadian Light Source, which is supported by the Canada Foundation for Innovation, Natural Sciences and Engineering Research Council of Canada, the University of Saskatchewan, the Government of Saskatchewan, Western Economic Diversification Canada, the National Research Council Canada, and the Canadian Institutes of Health Research.

▪ REFERENCES

(1) Nieminen, T. M.; Ukonmaanaho, L.; Rausch, N.; and Shotyk, W. Biogeochemistry of nickel and its release into the environment. In *Met. Ions Life Sci.* ***2007****, 2, 1–30.*
(2) Denkhaus, E. and Salnikow, K. Nickel essentiality, toxicity, and carcinogenicity. *Crit. Rev. Oncol. Hematol.* ***2002****, 42, 35-56.*
(3) Kasprzak, K. S.; Sunderman, F. W.; and Salnikow, K. Nickel carcinogenesis. *Mutat. Res.* ***2003****, 533, 67–97.*
(4) Schaumlöffel, D. Nickel species: analysis and toxic effects. *J. Trace Elem. Med. Biol.* ***2012****, 26 (1), 1-6.*
(5) Das, K. K.; Reddy, R. C.; Bagoji, I. B.; Das, S.; Bagali, S.; Mullur, L.; Khodnapur, J. P.; and Biradar M. S. Primary concept of nickel toxicity – an overview. *J. Basic Clin. Physiol. Pharmacol.* ***2019****, 30 (2), 141-152.*
(6) Lewis, A. E. Review of metal sulphide precipitation. *Hydrometallurgy* ***2010****, 104, 222–234.*
(7) Lewis, A. and van Hille, R. An exploration into the sulphide precipitation method and its effect on metal sulphide removal. *Hydrometallurgy* ***2006****, 81 (3-4), 197-204.*
(8) Ferris, F.G.; Fyfe, W.S.; and Beveridge, T.J. Bacteria as nucleation sites for authigenic minerals in a metal-contaminated lake sediment. *Chem Geol.* ***1987****, 63, 225–232.*
(9) Fortin, D.; Southam, G.; Beveridge, and T. J. Nickel sulfide, iron-nickel sulfide and iron sulfide precipitation by a newly isolated *Desulfotomaculum* species and its relation to nickel resistance. *Microb. Ecol.* ***1994****, 14, 121-132.*
(10) Sitte, J.; Pollok, K.; Langenhorst, F.; and Küsel, K. Nanocrystalline nickel and cobalt sulfides formed by a heavy metal-tolerant, sulfate-reducing enrichment culture. *Geomicrobiol. J.* ***2013****, 30, 36–47.*
(11) Qian, J.; Zhu, X.; Tao, Y.; Zhou, Y.; He, X.; and Li, D. Promotion of Ni^{2+} removal by masking toxicity to sulfate-reducing bacteria: Addition of citrate. *Int. J. Mol. Sci.* ***2015****, 16, 7932-7943.*
(12) Mokone, T. P.; van Hille, R.; and Lewis A. E. Metal sulphides from wastewater: Assessing the impact of supersaturation control strategies. *Water Res.* ***2012****, 46, 2088-2100.*
(13) Mansor, M.; Winkler, C.; Hochella Jr., M. F.; and Xu, J. Nanoparticulate nickel-hosting phases in sulfidic environments: Effects of ferrous iron and bacterial presence on mineral formation mechanism and solid-phase nickel distribution. *Front. Earth Sci.* ***2019****, 7, 151.*
(14) Huang, S.; Harris, K. D. M.; Lopez-Capel, E.; Manning, D. A. C.; and Rickard, D. "Amorphous nickel sulfide" is hydrated nanocrystalline NiS with a core-shell structure. *Inorg. Chem.* ***2009****, 48, 11486–11488.*

(15) Jeong, Y. U. and Manthiram, A. Synthesis of nickel sulfides in aqueous solutions using sodium dithionite. *Inorg. Chem.* ***2001****, 40, 73–77.*
(16) Wilkin, R. T. and Rogers, D. A. Nickel sulfide formation at low temperature: initial precipitates, solubility, and transformation products. *Environ. Chem.* ***2010****, 7, 514–523.*
(17) Balayeva, O. O; Azizova, A. A; Muradovb, M. B; Maharramova, A. M.; Eyvazovab, G. M.; Alosmanova, R. M.; Mamiyevc, Z. Q.; and Aghamaliyev Z. A. β-NiS and Ni_3S_4 nanostructures: Fabrication and characterization. *Mater. Res. Bull.* ***2016****, 75, 155-161*.
(18) Barim, G.; Smock, S. R.; Antunez, P. D.; Glaser, D.; and Brutchey, R. L. Phase control in the colloidal synthesis of well-defined nickel sulfide nanocrystals. *Nanoscale,* ***2018****, 10, 16298-16306.*
(19) Olivas, A.; Cruz-Reyes, J.; Petranovski, V.; Avalos, M.; and Fuentes, S. Synthesis and characterization of nickel sulfide catalysts. *J. Vac. Sci. Technol.* ***1998****, 16, 3515-3520.*
(20) Gramp, J. P.; Bigham, J. M.; Sasaki, K.; and Tuovinen, O. H. Formation of Ni- and Zn-sulfides in cultures of sulfate-reducing bacteria. *Geomicrobiol. J.* ***2007****, 24, 609–614.*
(21) Blowes, D. W.; Ptacek, C. J.; Benner, S. G.; McRae, C. W. T.; Bennett, T. A. and Puls R. W. Treatment of inorganic contaminants using permeable reactive barriers. *J. Contam. Hydrol.* ***2000****, 45, 123–137.*
(22) Huisman, J. L.; Schouten, G.; and Schultz, C. Biologically produced sulphide for purification of process streams, effluent treatment and recovery of metals in the metal and mining industry. *Hydrometallurgy* ***2006****, 83, 106-113.*
(23) Benner, S. G.; Blowes, D. W.; and Ptacek, C. J. A full-scale porous reactive wall for prevention of acid mine drainage. *Ground Water Monit. R.* ***1997****, 17 (4), 99–107.*
(24) Benner, S. G.; Blowes, D. W.; Gould, W. D.; Herbert, R. B.; Ptacek, C. J.; and Herbert, R. Geochemistry of a permeable reactive barrier for metals and acid mine drainage. *Environ. Sci. Technol.* ***1999****, 33 (16), 2793–2799.*
(25) Benner, S. G.; Blowes, D. W.; Ptacek, C. J.; and Mayer, K. U. Rates of sulfate reduction and metal sulfide precipitation in a permeable reactive barrier. *Appl. Geochem.* ***2002****, 17 (3), 301–320.*
(26) Wiederhold, J. G. Metal stable isotope signatures as tracers in environmental geochemistry. *Environ. Sci. Technol.* ***2015****, 49, 2606–2624.*
(27) Komárek, M.; Ratié, G.; Vaňková, Z.; Šípková, A.; and Vladislav Chrastný V. Metal isotope complexation with environmentally relevant surfaces: Opening the isotope fractionation black box. *Crit. Rev. Environ. Sci. Technol*. **2021**. DOI: 10.1080/10643389.2021.1955601
(28) Viers, J.; Grande, J. A.; Zouiten, C.; Freydier, R.; Masbou, J.; Valente, T.; de la Torre, M-L.; Destrigneville, C.; and Pokrovsky O. S. Are Cu isotopes a useful tool to trace metal sources and processes in acid mine drainage (AMD) context? *Chemosphere* ***2018****, 193, 1071-1079.*
(29) Yang, W-J.; Ding, K-B.; Zhang, P.; Qiu, H.; Cloquet, C.; Wen, H-J.; Morel, J-L.; Qiu, R-L; and Tang, Y-T. Cadmium stable isotope variation in a mountain area impacted by acid mine drainage. *Sci. Total Environ.* ***2019****, 646, 696-703.*
(30) Chételat, J.; Nielsen, S. G.; Auro, M.; Carpenter, D.; Mundy, L.; and Thomas, P. J. Vanadium stable isotopes in biota of terrestrial and aquatic food chains. *Environ. Sci. Technol*. ***2021,*** *55 (8), 4813-4821.*
(31) Gou, W.; Li, W.; Ji, J.; and Li, W. Zinc isotope fractionation during sorption onto Al oxides: atomic level understanding from EXAFS. *Environ. Sci. Technol*. ***2018****, 52 (16), 9087-9096.*
(32) Gourgiotis, A.; Mangeret, A.; Manhès, G.; Blanchart, P.; Stetten, L.; Morin, G.; Le Pape, P.; Lefebvre, P.; Le Coz, M.; and Cazala C. New insights into Pb isotope fingerprinting of U-mine material dissemination in the environment: Pb isotopes as a memory dissemination tracer. *Environ. Sci. Technol*. ***2020****, 54 (2), 797-806.*

(33) Cameron, V.; Vance, D.; Archer, C.; and House, C. H. A biomarker based on the stable isotopes of nickel. *Proc. Natl. Acad. Sci.* ***2009****, 106, 10944–10948.*
(34) Estrade, N.; Cloquet, C.; Echevarria, G.; Sterckeman, T.; Deng, T.; Tang, Y.; and Morel, J. L. Weathering and vegetation controls on nickel isotope fractionation in surface ultramafic environments (Albania). *Earth Planet. Sci. Lett.* ***2015****, 423, 24–35.*
(35) Ratié, G.; Quantin, C.; De Freitas, M. A.; Echevarria, G.; Ponzevera, E.; and Garnier, J. The behavior of nickel isotopes at the biogeochemical interface between ultramafic soils and Ni accumulator species. *J. Geochem. Explor.* ***2019****, 196, 182-191.*
(36) Ratié, G.; Jouvin, D.; Garnier, J.; Rouxel, O.; Miska, S.; Guimaraes, E.; Cruz Vieira, L.; Sivry, Y.; Zelano, I.; Montarges-Pelletier, E.; Thil, F.; and Quantin, C. Nickel isotope fractionation during tropical weathering of ultramafic rocks. *Chem. Geol.* ***2015****, 402 (0), 68–76.*
(37) Ratié, G.; Garnier, J.; Calmels; D.; Vantelon, D.; Guimarães, E.; Monvoisin, G.; Nouet, J.; Ponzevera, E.; and Quantin, C. Nickel distribution and isotopic fractionation in a Brazilian lateritic regolith: Coupling Ni isotopes and Ni K-edge XANES. *Geochim. Cosmochim. Acta* ***2018****, 230, 137-154.*
(38) Spivak-Birndorf, L. J.; Wang, S.; Bish, D. L.; Wasylenki, L. E. Nickel isotope fractionation during continental weathering. *Chem. Geol.,* ***2018****, 476, 316-326.*
(39) Wasylenki, L. E.; Howe, H. D.; Spivak-Birndorf, L. J.; and Bish, D. L. Ni isotope fractionation during sorption to ferrihydrite: implications for Ni in banded iron formations. *Chem. Geol.* ***2015****, 400 (0), 56–64.*
(40) Wang, S. J. and Wasylenki, L. E. Experimental constraints on reconstruction of Archean seawater Ni isotopic composition from banded iron formations. *Geochim. Cosmochim. Acta.* ***2017****, 206, 137–150.*
(41) Gueguen, B.; Sorensen, J. V.; Lalonde, S. V.; Peña, J.; Toner; B. M.; and Rouxel, O. Variable Ni isotope fractionation between Fe-oxyhydroxides and implications for the use of Ni isotopes as geochemical tracers. *Chem. Geol.* ***2018****, 481, 38-52.*
(42) Castillo Alvarez, C.; Quitté, G.; Schott, J.; and Oelkers, E. H. Experimental determination of Ni isotope fractionation during Ni adsorption from an aqueous fluid onto calcite surfaces. *Geochim. Cosmochim. Acta* ***2020****, 273, 26–36*.
(43) Sorensen, J. V.; Gueguen, B.; Stewart, B. D.; Peña, J.; Rouxel, O.; and Toner, B. M. Large nickel isotope fractionation caused by surface complexation reactions with hexagonal birnessite. *Chem. Geol.* ***2020****, 537, 119481*.
(44) Parigi, R.; Chen, N.; Reid, J.W.; Ptacek, C.J.; and Blowes, D.W. Nickel isotope fractionation during precipitation of Ni secondary minerals and synchrotron-based analysis of the precipitates. *Geochim. Cosmochim. Acta* ***2022****, 317, 91-105.*
(45) Postgate, J.R. The Sulfate-Reducing Bacteria. 2nd Edition, Cambridge University Press, Cambridge, United Kingdom, **1984**.
(46) Siebert, C.; Nägler, T. F.; and Kramers, J. D. Determination of molybdenum isotope fractionation by double-spike multicollector inductively coupled plasma mass spectrometry. Geochem. Geophys. Geosyst. ***2001****, 2,* DOI: 10.1029/2000GC000124.
(47) Gueguen, B.; Rouxel, O.; Ponzevera, E.; Bekker, A.; and Fouquet Y. Nickel isotope variations in terrestrial silicate rocks and geological reference materials measured by MC-ICP-MS. *Geostand. Geoanalytical Res.* ***2013****, 37, 297–317.*
(48) Ciscato, E. R.; Bontognali, T. R. R;. and Vance D. Nickel and its isotopes in organic-rich sediments: Implications for oceanic budgets and a potential record of ancient seawater. *Earth Planet. Sci. Lett.* ***2018****, 494, 239-250.*
(49) Wang, R. M.; Archer, C.; Bowie, A. R.; and Vance, D. Zinc and nickel isotopes in seawater from the Indian Sector of the Southern Ocean: The impact of natural iron fertilization versus Southern Ocean hydrography and biogeochemistry. *Chem. Geol.* ***2019****, 511, 452-464*.

(50) Fodje, M.; Grochulski, P.; Janzen, K.; Labiuk, S.; Gorin, J.; and Berg, R. 08B1-1: an automated beamline for macromolecular crystallography experiments at the Canadian Light Source *J. Synchrotron Rad.* ***2014****, 21, 633–637.*
(51) Toby, B. H. and Von Dreele, R. B. GSAS II: the genesis of a modern open-source all-purpose crystallography software package. *J. Appl. Crystallogr.* ***2013****, 46, 544–549.*
(52) ICDD (2019). PDF-4 + 2019 (Database). Edited by Dr. S. Kabekkodu. (International Centre for Diffraction Data, Newtown Square, PA, USA).
(53) Huang, S. Nanoparticulate Nickel Sulfide. Ph.D. Dissertation, Cardiff University, Cardiff, Wales, **2008**.
(54) Xu, J.; Murayama, M.; Roco, C. M.; Veeramani H., Michel M.; Rimstidt, J. D.; Winkler, C.; and Hochella Jr., M. F. Highly-defective nanocrystals of ZnS formed via dissimilatory bacterial sulfate reduction: A comparative study with their abiogenic analogues. *Geochim. Cosmochim. Acta.* ***2016****, 180, 1-14.*
(55) Mansor, M.; Berti D.; Hochella Jr., M. F.; Murayama, M.; and Xu, J. Phase, morphology, elemental composition, and formation mechanisms of biogenic and abiogenic Fe-Cu-sulfide nanoparticles: A comparative study on their occurrences under anoxic conditions. *Am. Mineral.* ***2019***, *104, 703–717.*
(56) Konhauser, K. O. and Urrutia, M. M. Bacterial clay authigenesis: a common biogeochemical process. *Chem. Geol.* ***1999****, 161, 399–413.*
(57) Tazaki, K. Microbial formation of a halloysite-like mineral. *Clays Clay Miner.* ***2005****, 53, 224–233.*
(58) Fiore, S.; Dumontet, S.; Huertas, J.; and Pasquale, V. Bacteria-induced crystallization of kaolinite. *Appl. Clay Sci.* ***2011****, 53, 566–571.*
(59) Singh, R.; Paul, D.; and Jain, R. K. Biofilms: Implications in bioremediation. *Trends Microbiol.* ***2006****, 14 (9), 389-397.*
(60) Kumar, M. and Pakshirajan, K. Novel insights into mechanism of biometal recovery from wastewater by sulfate reduction and its application in pollutant removal. *Environ. Technol. Innov.* ***2020****, 17, 100542.*
(61) Castillo, J.; Perez-Lopez, R.; Caraballo, M. A.; Nieto, J. M.; Martins, M.; Costa, M. C.; Olias, M.; Ceron, J. C.; and Tucoulou, R. Biologically-induced precipitation of sphalerite-wurtzite nanoparticles by sulfate-reducing bacteria: Implications for acid mine drainage treatment. *Sci. Total Environ.* ***2012****, 423, 176–184.*
(62) Deng, X.; Dohmae, N.; Kaksonen, A. H.; and Okamoto, A. Biogenic iron sulfide nanoparticles to enable extracellular electron uptake in sulfate-reducing bacteria. *Angewandte Chemie* ***2020***, *132.15, 6051-6055*.
(63) Mansor, M. and Xu, J. Benefits at the nanoscale: a review of nanoparticle-enabled processes favouring microbial growth and functionality. *Environmental Microbiology* ***2020****, 22 (9), 3633–3649.*
(64) Fujii, T.; Moynier, F.; Dauphas, N.; and Abe, M. Theoretical and experimental investigation of nickel isotopic fractionation in species relevant to modern and ancient oceans. *Geochim. Cosmochim. Acta* ***2011****, 75 (2), 469–482*.
(65) Fujii, T.; Moynier, F.; Blichert-Toft, J.; and Albarède, F. Density functional theory estimation of isotope fractionation of Fe, Ni, Cu and Zn among species relevant to geochemical and biological environments. *Geochim. Cosmochim. Acta* ***2014****, 140, 553–576.*
(66) Vance, D.; Little, S. H; Archer, C.; Cameron, V.; Andersen, M. B.; Rijkenberg, M. J. A.; and Lyson T. W. The oceanic budgets of nickel and zinc isotopes: The importance of sulfidic environments as illustrated by the Black Sea. *Phil. Trans. R. Soc. A.* ***2016***, *374, 20150294.*
(67) Liu, S.; Li, Y.; Ju, Y.; Liu, J.; Liu, J.; and Shi, Y. Equilibrium nickel isotope fractionation in nickel sulfide minerals. *Geochim. Cosmochim. Acta* ***2018****, 222, 1–16.*